



Upstream satellite remote sensing for river discharge forecasting: Application to major rivers in South Asia

Feyera A. Hirpa^a, Thomas M. Hopson^{b,*}, Tom De Groeve^c, G. Robert Brakenridge^d, Mekonnen Gebremichael^a, Pedro J. Restrepo^e

^a Department of Civil & Environmental Engineering, University of Connecticut, Storrs, CT 06269, USA

^b Research Applications Laboratory, National Center for Atmospheric Research, Boulder, CO 80307-3000, USA

^c Joint Research Centre of the European Commission, Ispra, Via Fermi 2147, 21020 Ispra, Italy

^d CSDMS, INSTAAR, University of Colorado, Boulder, CO 80309-0450, USA

^e North Central River Forecast Center, NOAA, Chanhassen, MN, 55317, USA

ARTICLE INFO

Article history:

Received 19 August 2011

Received in revised form 16 November 2012

Accepted 17 November 2012

Available online xxxx

Keywords:

Floods

Forecasting

Flow estimation

Flood wave

Wave speed

ABSTRACT

In this work we demonstrate the utility of satellite remote sensing for river discharge nowcasting and forecasting for two major rivers, the Ganges and Brahmaputra, in southern Asia. Passive microwave sensing of the river and floodplain at more than twenty locations upstream of Hardinge Bridge (Ganges) and Bahadurabad (Brahmaputra) gauging stations are used to: 1) examine the capability of remotely sensed flow information to track the downstream propagation of river flow waves and 2) evaluate their use in producing river flow nowcasts, and forecasts at 1–15 days lead time. The pattern of correlation between upstream satellite data and in situ observations of downstream discharge is used to estimate wave propagation time. This pattern of correlation is combined with a cross-validation method to select the satellite sites that produce the most accurate river discharge estimates in a lagged regression model. The results show that the well-correlated satellite-derived flow (SDF) signals were able to detect the propagation of a river flow wave along both river channels. The daily river discharge (contemporaneous) nowcast produced from the upstream SDFs could be used to provide missing data estimates given its Nash–Sutcliffe coefficient of 0.8 for both rivers; and forecasts have considerably better skill than autoregressive moving-average (ARMA) model beyond 3-day lead time for Brahmaputra. Due to the expected better accuracy of the SDF for detecting large flows, the forecast error is found to be lower for high flows compared to low flows. Overall, we conclude that satellite-based flow estimates are a useful source of dynamical surface water information in data-scarce regions and that they could be used for model calibration and data assimilation purposes in near-time hydrologic forecast applications.

© 2012 Elsevier Inc. All rights reserved.

1. Introduction

River flow measurements are critical for hydrological data assimilation and model calibration in flood forecasting and other water resource management issues. In many parts of the world, however, in situ river discharge measurements are either completely unavailable or are difficult to access for timely use in operational flood forecasting and disaster mitigation. In such regions, flood inundation information derived from microwave remote sensors (e.g. Birkinshaw et al., 2010; Bjerklie et al., 2005; Brakenridge et al., 2005, 2007, 1998; De Groeve, 2010; Smith, 1997; Smith & Pavelsky, 2008 and Temimi et al., 2005) or surface

water elevation estimated from satellite altimetry (e.g. Alsdorf et al., 2000, 2001; Birkett, 1998; Jung et al., 2010) could be used as alternative sources of surface water information for hydrologic applications.

Brakenridge et al. (2007) demonstrate, through testing over different climatic regions of the world, including rivers in the United States, Europe, Asia and Africa, that satellite passive microwave data can be used to estimate river discharge changes, river ice status, and watershed runoff. The data were obtained by the Advanced Microwave Scanning Radiometer–Earth Observing System (AMSR-E) aboard NASA's Aqua satellite. The method uses the large difference in 36.5 GHz (14 × 8 km spatial resolution), H-polarized, night-time “brightness temperature” (upwelling radiance) between water and land to estimate the in-pixel proportion of land to water, on a near-daily basis over a period of more than 10 years. The measurement pixels are centered over rivers, and are calibrated by nearby reference pixels over dry land to remove other factors affecting microwave emission (a ratio is calculated). The resulting signal is very sensitive to small changes in river discharge for all ranges of the moisture content in the calibration pixel.

* Corresponding author. Tel.: +1 303 497 2706; fax: +1 303 497 8401.

E-mail addresses: fah07002@engr.uconn.edu (F.A. Hirpa), hopson@ucar.edu (T.M. Hopson), tom-de-groev@jrc.ec.europa.eu (T. De Groeve), robert.brakenridge@colorado.edu (G.R. Brakenridge), mekonnen@engr.uconn.edu (M. Gebremichael), Pedro.Restrepo@noaa.gov (P.J. Restrepo).

Using the same data from AMSR-E, De Groeve et al. (2006) provide a method to detect major global floods on a near-real time basis. De Groeve (2010) shows in Namibia, southern Africa, that the passive microwave based flood extent corresponds well with observed flood hydrographs in monitoring stations where the river overflows the bank. It was also noted that the signal to noise ratio is highly affected by variable local conditions on the ground (De Groeve, 2010), such as the river bank geometry and the extent of flood inundation. For example, in cases of confined flows, the river stays in the banks and hence the change in river discharge mainly results in water level variation without producing much difference in river width.

Upper-catchment satellite based flow monitoring may provide major improvements to river flow forecast accuracy downstream, primarily in the developing nations where there is a limited availability of ground based river discharge measurements. Bangladesh is one such case where river flooding has historically been a very significant problem to socioeconomic and public health. Major flooding occurs in Bangladesh with a return period of 4–5 years (Hopson & Webster, 2010) caused by the Ganges and Brahmaputra Rivers, which enter into the country from India, and join in the Bangladeshi low lands. Because of limited river discharge data sharing between the two countries, the only reliable river streamflow data for Bangladesh flood prediction is from sites within the national borders, and this has traditionally limited forecast lead-times to 2 to 3 days in the interior of the country.

Several water elevation and discharge estimation attempts have been made based on satellite altimetry for the Ganges and Brahmaputra rivers. Jung et al., 2010 used satellite altimetry from Shuttle Radar Topography Mission digital elevation model (SRTM DEM) to estimate water elevation and slope for Brahmaputra River. The same study also applied Manning's equation to estimate discharge from the water surface slope and Woldemichael et al. (2010) later improved the discharge estimation error through better selection of hydraulic parameters and Manning's roughness coefficient. Siddique-E-Akbor et al. (2011) compared the water elevation derived from Envisat satellite altimetry with simulated water levels by HEC-RAS model for three rivers in Bangladesh, in which they reported the average (over 2 years) root mean square difference of 2.0 m between the simulated and the satellite based water level estimates.

In another study, Papa et al. (2010) produced estimates of monthly discharges for the Ganges and Brahmaputra rivers using TOPEX-Poseidon (T-P), ERS-2, and ENVISAT satellite altimetry information. Such monthly and seasonal discharge estimates are important for weather and climate applications, but shorter time scale information is also needed, such as daily or hourly, for operational short term river flow forecasting. However, the use of altimetry data is currently temporally sampling rate limited to a 10 day repeat cycle (T-P) or a 35 day repeat cycle (ER-2/ENVISAT). Biancamaria et al. (2011) also used T-P satellite altimetry measurements of water level at upstream locations in India to forecast water levels for Ganges and Brahmaputra rivers after they cross the India–Bangladesh border. The same paper also suggests that “... the forecast might even be improved using ancillary satellite data, such as precipitation or river width estimates” (Biancamaria et al., 2011, p.5).

The current study uses multiple upstream estimates of the river width (area covered by river reach) along the main river channels to forecast discharge at downstream locations. Specifically, we examine the utility of using passive microwave derived river width estimates for near-real time river flow estimation and forecasting for the Ganges and Brahmaputra rivers after they cross India/Bangladesh Border. One of the advantages of using passive microwave signal is that the sensors do not suffer very much from cloud interference; another is that they are very much more frequent than any available altimetry (river stage) information. Limitation of discharge estimation from remotely sensed river width is the relatively small change in river width at some locations even when there is significant in-channel discharge changes (Brakenridge et al., 2007) To overcome this problem, measurement

locations should be chosen carefully to maximize sensitivity of width to discharge fluctuation.

The following has two parts. First, we investigate directly the use of satellite-derived flow signal (SDF) data produced by the Global Flood Detection System of the GDACS (Global Disaster and Alert Coordination System, Joint Research Center-Ispra, European Commission) for tracking river flow wave propagation along the Ganges and Brahmaputra. These data are available to the public at: <http://old.gdacs.org/flooddetection/>; see also Kugler and De Groeve, 2007 pdf file enclosed, from <http://floodobservatory.colorado.edu/GlobalFloodDetectionSystem.pdf>. SDF information is, as noted, the ratio of the brightness temperature of nearby land pixels, outside of the reach of the river, to the brightness temperature of the measurement pixel (centered at the river). The second part of the study uses the SDF information for river flow simulation and forecasting in Bangladesh. The SDF is also combined with persistence to assess the degree of forecast improvement compared to persistence and Autoregressive moving-average (ARMA) model forecast. The discharge forecast has also been converted to water level and compared to in-situ river stage measurements. The simulations and forecasts are compared against ground based discharge measurements. The details of data used are described in Section 2. Section 3 presents the results of the flow signal analysis, the variable selection method is described in Section 4, and then the results of discharge nowcasting and forecasting in Section 5. Section 6 summarizes the water level forecast results.

2. Study region and data sets

2.1. Study region

The study areas are the Ganges and Brahmaputra river basins in south Asia (see Fig. 1). These are transboundary Rivers which join in lowland Bangladesh after crossing the India–Bangladesh border. There is substantial need for accurate and timely river flow forecast in Bangladesh. For example, according to estimates (CEGIS, 2006a, 2006b; RIMES, 2008; Hopson & Webster, 2010), an accurate 7 day forecast has the potential of reducing post-flood costs by as much as 20% over a cost reduction of 3% achieved with just a two-day forecast. Beginning in 2003, Hopson and Webster (2010) developed and successfully implemented a real-time probabilistic forecast system for severe flooding for both the Ganges and Brahmaputra in Bangladesh. This system triggered early evacuation of people and livestock during the 2007 severe flooding along the Brahmaputra. Although the forecast system shows useful skill out to 10-day lead-times by utilizing satellite-derived TRMM (Huffman et al., 2005, 2007) and CMORPH (Joyce et al., 2004) precipitation estimates and ensemble weather forecasts from the European Center for Medium Weather Forecasts (ECMWF), Hopson and Webster (2010) also indicate that the accuracy of the forecasts could be significantly improved if flow measurements higher upstream in the catchments were available. The limited in-situ data sharing between Bangladesh and the upstream countries makes the remotely sensed water data the most useful.

It should also be noted that impoundments and diversions of the river flows between remotely-sensed measurement locations would lessen the predictability of the approach presented in this paper. However, as discussed further in Hopson and Webster (2010), The Brahmaputra has yet (as of the most recent data period in this study) to have a major hydraulic structure built along its course (Singh et al., 2004) and as such, it can be modeled as a naturalized river. For the water diversions along the Ganges, these structures were designed primarily for use in the dry season and not during the monsoonal flood season. On the basis of an additional study by Jian et al. (2009) and the Flood Forecasting and Warning Centre (FFWC, 2000, personal communication), it is assumed the major diversions do not affect discharge into Bangladesh beyond 15 June. However, Ganges dry season low flow predictability may be impacted, a topic we will return to this later in Section 6 of this study.

2.2. Data sets

The Joint Research Center (JRC-Ispira, <http://www.gdacs.org/floodmerge/>), in collaboration with the Dartmouth Flood Observatory (DFO) (<http://www.dartmouth.edu/~floods/>) produces daily near real-time river flow signals, along with flood maps and animations, at more than 10,000 monitoring locations for major rivers globally (GDACS, 2011). For details of the methodology used to extract the daily signals from the passive microwave remote sensing (the American and Japanese AMSR-E and TRMM sensors), the reader is referred to De Groeve (2010) and Brakenridge et al. (2007). In this study, we use the daily SDF signals along the Ganges and Brahmaputra river channels provided by the JRC. The river flow signals are available starting from December 8, 1997 to the present. Data from a total of 22 geolocated sites ranging between an upstream distances from the outlet of 63 to 1828 km were analyzed for the Ganges, and 23 geolocated sites with a range of 53 to 2443 km were used for the Brahmaputra. Further details of these data are presented in Table 1.

Water level observations for the Ganges River at Hardinge Bridge and the Brahmaputra River at Bahadurabad (Fig. 1) were obtained from the Flood Forecasting and Warning Center (FFWC) of the Bangladesh Water Development Board. We also used daily rating curve-derived gauged discharge from December 8, 1997 to December 31, 2010 for model training and validation purposes. See Hopson and Webster (2010) for further details on the rating curve derivations.

3. Satellite-derived flow signals

3.1. Correlation with gauge observations

Fig. 2a and b shows correlations between three SDF estimates and gauge discharge observations at Hardinge Bridge (Ganges) and Bahadurabad (Brahmaputra) versus lag time, respectively, and with the correlation maxima shown by solid circles on the figures. The within-channel distances between the locations where the upstream SDF were measured and the outlet of the watershed have also been indicated in the figures. The variation of correlations with lag time has different characteristics depending on the flow path length (FPL, the hydrologic distance between the SDF detection site and the outlet). Specifically, for shorter FPL the correlation decreases monotonically with increasing lag time; however, for longer FPL the correlation initially increases to reach a maximum value, and then decreases with increasing lag time. This lag of the correlation pattern (in this case, shifting of the maximum with FPL) is in agreement with the fact that river flow waves take a longer time for the furthest FPL to propagate from upstream location to the downstream outlet. The time at which maximum correlation occurs is an approximate estimate of the flow time.

3.2. Variation of flow time with flow path length

We estimate the travel time from the correlation pattern of the SDFs by assuming that the lag time at which the maximum correlation

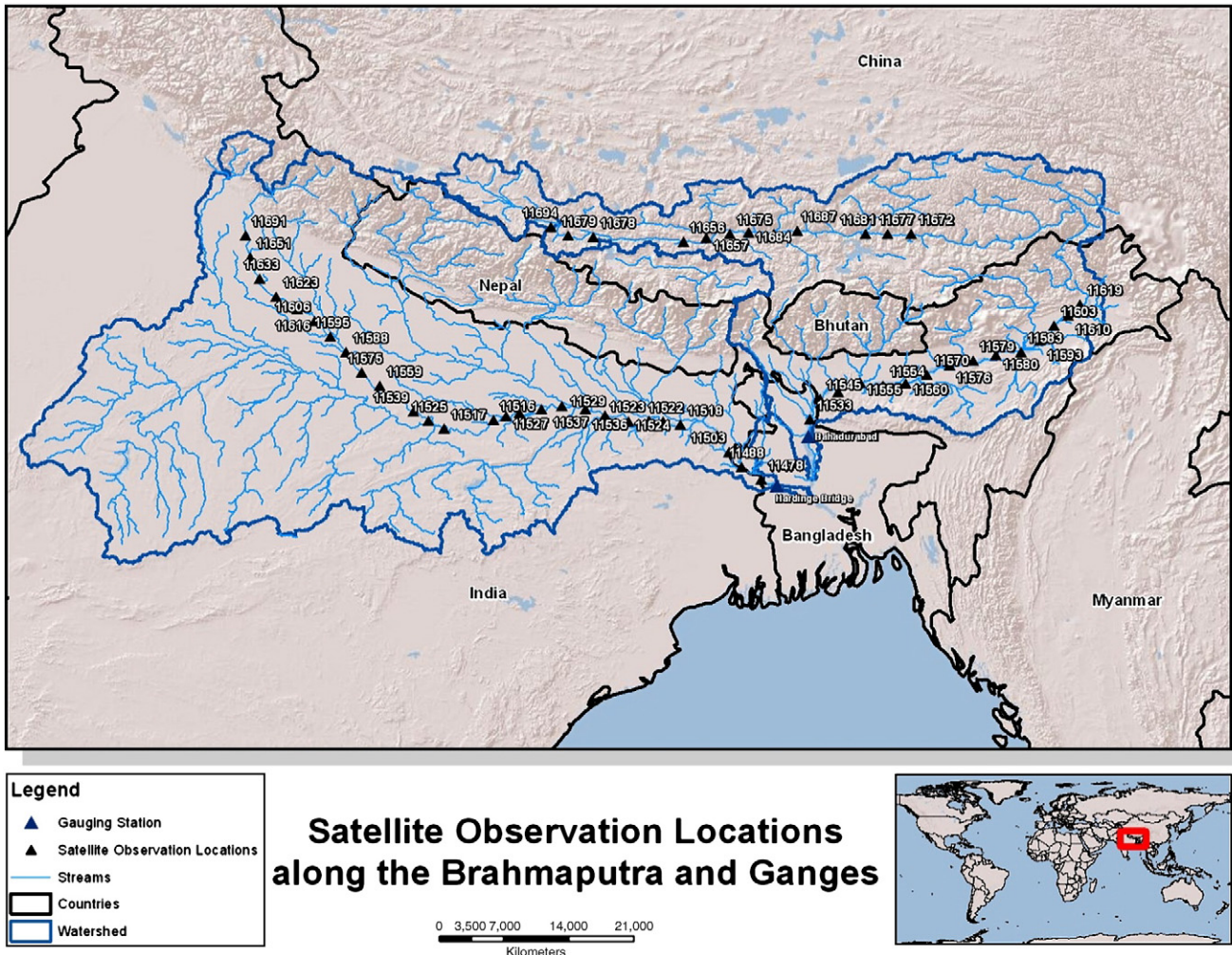


Fig. 1. The Brahmaputra and Ganges Rivers in South Asia. The satellite flood signal observations are located on the main streams of the Brahmaputra (top right) and the Ganges (bottom left) rivers. The observation sites are shown in small dark triangles and they are labeled by the GFDS site ID (see Table 1).

Table 1

Details of the satellite-derived flow signals (“MagnitudeAvg” in the GDACS database) used for the study. The site ID, latitude, longitude and flow path length (FPL) are provided. The period of record for all the data, including the satellite flood signals and the gauge discharge observations at Hardinge Bridge and Bahadurabad is December 8, 1997 to December 31, 2010.

Ganges Gauging location at Hardinge Bridge: 24.07N, 89.03E				Brahmaputra Gauging location at Bahadurabad: 25.09N, 89.67E				
	GFDS site ID	Latitude (N)	Longitude (E)	FPL (KM)	GFDS site ID	Latitude (N)	Longitude (E)	FPL (KM)
1	11478	24.209	88.699	63	11533	25.451	89.707	53
2	11488	24.469	88.290	121	11545	25.875	89.910	117
3	11518	25.341	87.030	340	11558	26.014	90.282	145
4	11522	25.402	86.670	370	11555	26.221	90.738	204
5	11523	25.415	86.379	420	11554	26.148	91.214	285
6	11524	25.409	85.950	550	11560	26.205	91.683	330
7	11536	25.660	85.069	650	11570	26.383	92.119	385
8	11537	25.722	84.587	676	11576	26.574	92.586	475
9	11532	25.672	84.150	690	11579	26.671	93.074	496
10	11528	25.585	83.700	725	11580	26.776	93.555	590
11	11527	25.513	83.430	800	11583	26.853	94.062	630
12	11539	25.620	81.519	1180	11593	27.089	94.456	660
13	11548	25.938	81.207	1220	11603	27.394	94.748	712
14	11559	26.149	80.815	1300	11610	27.603	95.040	750
15	11575	26.423	80.439	1320	11619	27.836	95.293	837
16	11588	26.852	80.123	1381	11677	29.296	91.305	1698
17	11595	27.179	79.786	1431	11681	29.300	90.854	1737
18	11606	27.494	79.470	1520	11687	29.369	89.441	1907
19	11616	27.738	79.110	1590	11685	29.295	88.966	1929
20	11623	28.003	78.674	1640	11684	29.334	88.443	1996
21	11651	28.812	78.131	1761	11675	29.303	88.049	2045
22	11691	29.259	78.035	1828	11678	29.232	85.230	2380
23					11679	29.267	84.709	2443

occurred is a proxy measure of the river flow wave celerity propagation time. The estimated flow time for each SDF is shown on Fig. 3a and b for the Ganges and Brahmaputra rivers respectively. In these figures, the flow time estimated from the river flow signals was plotted against its flow path length, where the flow path length is the hydrologic distance between the river flow signal detection sites to the observed gauging location of the watershed (e.g. Hardinge Bridge for the Ganges, and Bahadurabad for the Brahmaputra). We estimated the flow path length from a digital elevation map (DEM) of 90 m resolution obtained from the HydroSHEDS (Hydrological data and maps based on Shuttle Elevation Derivatives at multiple Scales) data.

If the river flow wave propagation speed were to be assumed constant, then the elapsed flow time should increase linearly with flow path length. However this is not strictly the case for both rivers in this study (see Fig. 3a and b). Instead, we observe variations of flow time with upstream distance. This should in fact be expected. Consider in the case of the Brahmaputra that the wave speed on the Tibetan plateau is probably higher than on the low-gradient plains of Bangladesh, and speeds are likely quite high as the river descends through steep gorges into Indian’s Assam State. As an example, the flow time appears less than or equal to 1 day for flow distances shorter than 750 km and 1000 km for the Ganges and Brahmaputra respectively; however the flow time appears to increase to more than 10 days for the Ganges at FPLs of 750 km and 7 days for the Brahmaputra at FPLs of 100 km. Other possible factors contributing to the inconsistent increase of the flow time with flow length are: the noise introduced by the local ground conditions (perhaps the most significant factor), unaccounted inflows generated between the satellite and ground based observation locations, intrinsic changes in the celerity of different magnitude flow waves, propagation time variations during times of lower base flow versus higher base flows, among others.

It should also be noted that there are considerable differences in propagation speed estimates between the Ganges and Brahmaputra rivers. For example, it appears to take 11 days for river flow waves to travel 1828 km distance (the furthest upstream point, 11691) along

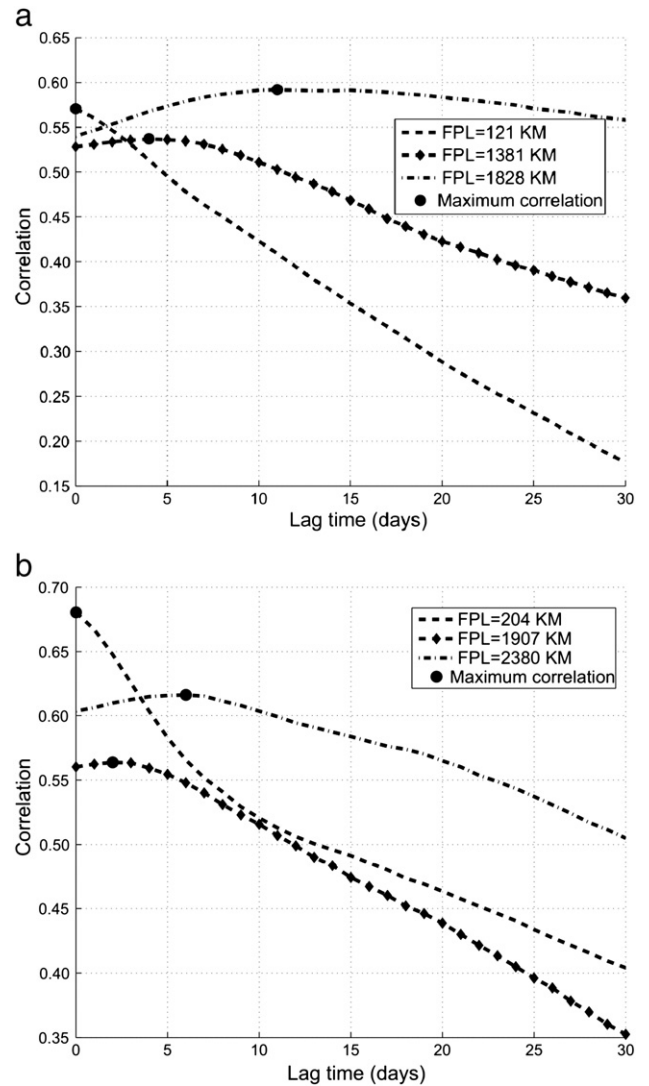


Fig. 2. a. Correlation versus lag time between daily in-situ streamflow and upstream satellite flood signals, SDFs (only 3 shown here) and gauge discharge at Hardinge Bridge along the Ganges River in Bangladesh. As expected, the lag time at which peak correlation occurs (shown as a dark dot) is greater for longer flow path lengths (FPL) from the gauge at Hardinge. b. Correlation versus lag time between daily in-situ streamflow and upstream satellite flood signals, SDFs (only 3 shown here) and gauge discharge at Bahadurabad along the Brahmaputra River.

the Ganges, whereas, for the Brahmaputra, only 2 days appear to be required for a comparable path length of 1907 km (site 11687).

Even under the expectation of differing wave celerity for different reaches of the same river, it is still informative to derive an approximate average propagation time over the majority of the length of the river course using the SDM data to see if these data produce an estimate in a physically-reasonable range. First, we note the correlation of flow time to flow path length estimates shown in Fig. 3a (Ganges) and b (Brahmaputra) are 0.78 and 0.66, respectively, and the correlations are statistically significant ($p < 0.01$). To estimate the celerity from these data, we constrain a regression fit through the origin (zero distance and zero flow time), and the inverse of the slope provides the celerity, giving $2.3 \leq 2.9 \leq 3.8$ m/s for the Ganges, and $7.5 \leq 9.6 \leq 13.5$ m/s for the Brahmaputra. However, because the strength of the original correlation differs for each of the data points shown in Fig. 3, as a check a weighted least-squares fit to the data was also performed, where the weights are given by the strength of the data point’s correlation. These latter results give only slightly different estimates of the mean celerity (with estimates and regression lines shown in Fig. 3). Also note

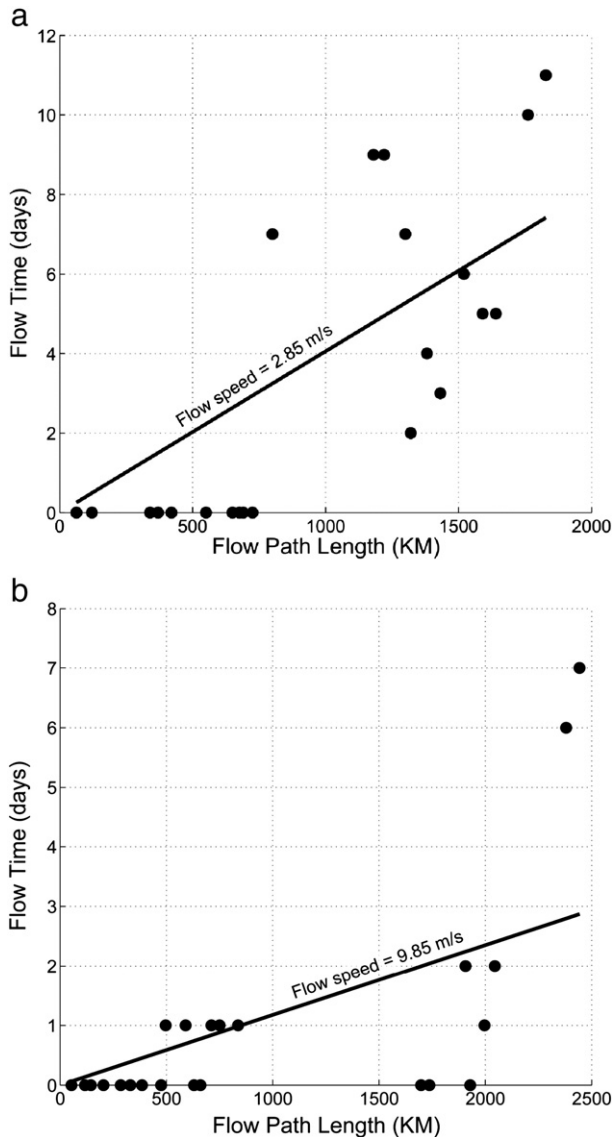


Fig. 3. a. Plot of flow time (as estimated from the satellite flood signal data) versus distance from the satellite flow detection point to the outlet (Hardinge bridge station) of the Ganges River. The flow time is the lag time at which the peak correlation occurred, as shown in Fig. 2a. The flow speed estimated from the slope of the fitted line is 2.9 m/s. b. Same as Fig. 3a, but for Brahmaputra river. The flow speed estimated from the slope of the fitted line is 9.6 m/s.

that the Brahmaputra celerity is estimated to be more than three times that of the Ganges, as anticipated given the Brahmaputra's steeper average channel slope. The elevation of Ganges drops only 225 m from the furthest upstream site ("11475") to the Hardinge Bridge over a flow distance of 1828 km, while that of Brahmaputra drops more than 3870 m for a comparable flow distance from site "11687" to Bahadurabad.

As a separate check, we would like to derive independent estimates for the wave propagation times estimated in Fig. 3. Both of these rivers have low gradients around the downstream gauging locations of interest, so it is anticipated that pressure gradient effects would need to be accounted for in estimating wave speeds around these locations. However, as discussed further in Hopson and Webster (2010), attempts to account for dynamic (and hysteresis) effects in the characterization of the depth and discharge relationship at the downstream gauging locations were not significant. So further noting that because both the discretization time of the satellite estimates is one day, and that also both channels' flow slowly varies in time, we expect that most of the low frequency channel width variations we have detected can at least

be approximated by kinematic wave theory. To estimate a range of possible wave propagation speeds, we use the derived rating curves for the downstream gauging locations, estimates for the range of channel widths, and the Kleitz–Seddon Law (Beven, 1979) for kinematic wave celerity c ,

$$c = \frac{1}{W} \frac{dQ}{dy} \quad (1)$$

where W is the channel top-width, Q the discharge, and y the river stage. For the Brahmaputra at Bahadurabad we estimate $4 \text{ m/s} < c < 8 \text{ m/s}$; for the Ganges at Hardinge Bridge we estimate $2 \text{ m/s} < c < 6 \text{ m/s}$. As with the satellite-derived signals, these estimates also show the wave propagation speeds of the Brahmaputra being greater than those of the Ganges, with its flatter channel slope. It should also be noted that the celerity estimated from the satellite-derived flow signals represents a total reach-length (i.e. FPL) average, while these kinematic wave speeds strictly apply only over the neighboring region of the gauging locations.

3.3. Limitations of the flow propagation model

Note that the accuracy of the simple model of wave celerity we have presented in the last section and shown in the regression lines of Fig. 3a and b, is based on the degree of which the source of the discharge is based in the upper catchments of the rivers, which then propagates downstream, with lagged positive correlations between upstream discharge estimates and the downstream gauging locations. In principal, however, sources of precipitation and thus river flow occur throughout the river catchment. As one such example, a significant portion of the Brahmaputra river basin's dry season flows stem from Himalayan snow melt up in the higher reaches of the catchment's Tibetan plateau, which would lead to a strengthening of the upstream–downstream discharge correlation. However, during the monsoon season, some of the largest sources of precipitation occur in the lower reaches of the catchment in the hills of India's Meghalaya state, bordering Bangladesh, containing the village of Mawsynram, one of the wettest locations on earth.

To investigate the influence of the location, spatial, and temporal scale of precipitation on the simple model for estimated flow propagation time shown in Fig. 3, we conducted a simple synthetic experiment where both the distribution, spatial size, and temporal length of rainfall over a saturated hypothetical watershed is varied, and then the excess rainfall is routed to the outlet using a linear reservoir unit hydrograph (Chow et al., 1988). In the synthetic experiment, the areal coverage (as a fraction of catchment area) of the precipitation, the location of the rainfall within the hypothetical watershed, and the length the precipitation persisted were varied to isolate the impacts of spatial and temporal scale and distribution on propagation time estimates. The results (not shown here) from this synthetic experiment do indeed indicate that variable precipitation distribution over the watershed affects the correlation between streamflow at multiple upstream locations and at the outlet, as one would expect. Interestingly, over our set of experiments there was no impact on the optimal lag in the correlation between two locations; however, in the presence of experimental noise, certain scenarios could lead to a more likely misdiagnosing of this lag. However, to systematically describe the influence of the precipitation scale on river flow wave propagation time, a separate and a more realistic experiment (beyond the scope of the current paper) with observed precipitation data over the river basin would be necessary.

4. Selection of satellite flow signals for discharge estimation

As presented in the previous sections, the SDF are well correlated to the daily ground discharge measurements and they also capture the propagation of river flow waves going downstream for the Ganges and Brahmaputra rivers. We used the SDF available upstream of the Hardinge Bridge (Ganges) and Bahadurabad (Brahmaputra) to produce

daily discharge nowcast and forecasts for 1–15 day lead times at the gauging stations.

To accomplish this, a cross-validation regression model is applied, in which the anomaly of SDF signals are used as a regression variable and the ground discharge observation anomaly at the outlet is used for training and validation purposes. The nowcasting/forecasting steps for each lead time increment are as follows:

- i. *Calculate the correlation map.* The correlation map is helpful for understanding the linear relationship between the SDF signals and the ground discharge observation. The variability of the correlation with lag time (as described in Section 3) can also be used to trace the river flow wave propagation. Another useful aspect of the correlation map is that it can be used as an indicator of the most relevant variables to be used in the discharge estimation model. All data sets have different correlations depending on the location, flow path length and lag time, indicating that the local ground condition, besides the place and time of observation, should be taken in to consideration before using the SDF for any application. All data sets do not have strong linear relationship with the ground observation and hence this step is useful for identifying the variables more related to the river flow measurement for the discharge estimation model to be used in the next steps. It should be noted that the correlation map calculated from anomalies is different from the map shown in Figs. 4a and b, which were calculated directly from observations before removing climatology.
- ii. *Sort the correlation in decreasing order.* Variables which are more correlated with ground discharge measurements will be used in the forecast model, thus to simplify the selection process, we sorted the correlations calculated (see Fig. 4) in step i before performing the selection task.
- iii. *Pick the variables to be used in the discharge estimation model and generate the river discharge.* We use a cross-validation approach to select variables, among the SDF signals at multiple sites, to be used in the model. Identifying the most relevant regression variables is required in order to prevent over fitting and thus to reduce the error in the estimated discharge. We select the best correlated river flow signals to the ground discharge observation as “the most relevant variables” to be used in the model. To determine the optimal number, we applied a ten-percent leave-out cross-validation model, where 10% of the data is left out (to be used for validation) at a time and a linear regression is fit to the remaining 90%. This is done repeatedly until each data point is left out, but no data point is used more than once for the validation purpose. This is followed by calculating the root mean square error (RMSE) of the validation sets. Finally, the number of variables that produced the smallest RMSE calculated over the whole out-of-sample data sets is considered as the optimal number to be used in the regression model. The variables selected for each lead time forecast have been shown in the Appendix (Figs. A1 and A2). The minimum RMSE criterion is simple to implement but it should be noted that this criteria might suffer from isolated extreme events (see Gupta et al., 2009).
- iv. *Repeat the steps ii–iii for all lead times.* We generated the river discharge nowcast and forecast for each lead time (1 to 15 days) by repeating the regression variable identification and discharge generation steps.

5. Results of discharge nowcasts and forecasts

5.1. Discharge nowcasts and forecasts using satellite river flow signals only

We use the cross-validation approach presented above to generate discharge nowcast (lead time of 0 days) and 1 to 15 days lead time forecast from the SDF signals detected at multiple points (see

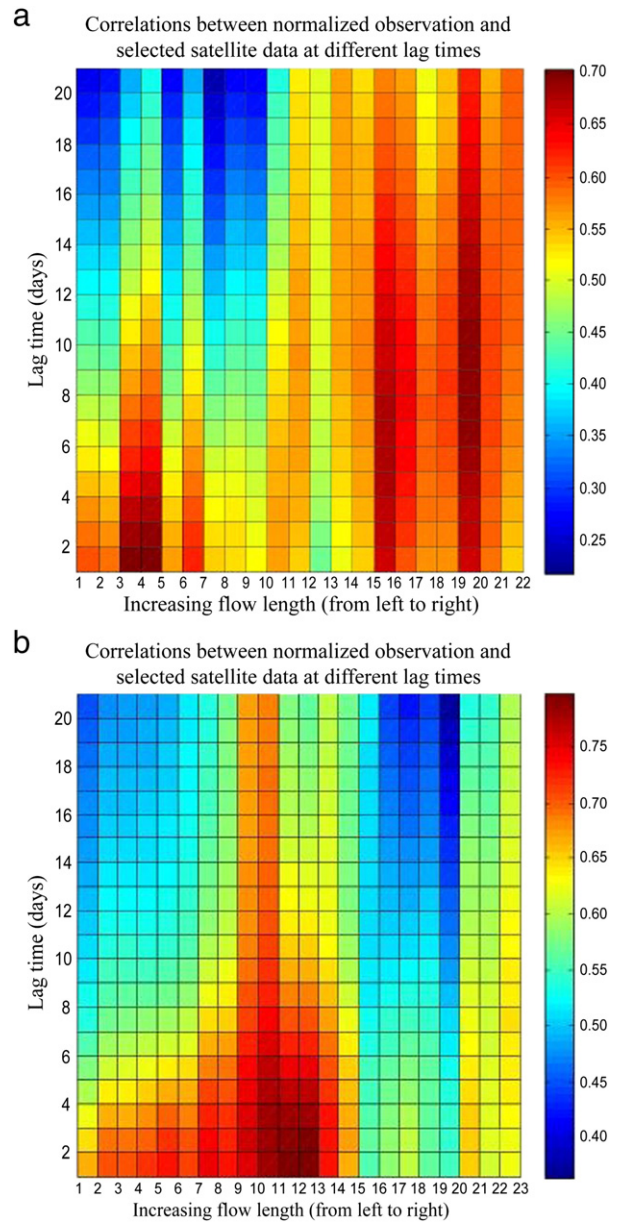


Fig. 4. a. Lagged correlation map of daily satellite-derived flow signals calculated against the discharge observation at Hardinge Bridge for Ganges River. The horizontal axis shows the satellite flood signal sites (see Fig. 1) arranged in the order of increasing flow path length and the vertical axis shows lag time (days). b. Same as Fig. 4a, but for Brahmaputra.

Table 1) upstream of the Hardinge Bridge (Ganges) and Bahadurabad (Brahmaputra). Past and current satellite river flow signals at several locations upstream of the forecast points were used as input to the forecasting model, and the rating curve-derived gauge discharge observations (December 8, 1997 to December 31, 2010) at the outlets were used for model training purpose. Fig. 5 shows time series plots of the discharge nowcast and 5- and 10-day forecasts overlaid on the gauge observations for Ganges River at the Hardinge Bridge (Figs. 5a and b) and Brahmaputra river at Bahadurabad (Figs. 5c and d) during a pair of selected monsoon flood years.

The discharge nowcast estimated from SDF captured fairly well the Ganges monsoonal flow of 2003 but with some underestimation of the peak flow of September 20, 2003 (see Fig. 5a). The rising and falling limbs of the discharge during the summer period also generally matched (with little fluctuations). Similarly, there is good agreement with the rising and falling sides of the flow for 2007 (see Fig. 5b), but

the highest peak is again underestimated by the SDF forecast. The SDF nowcasts for 2004 and 2007 Brahmaputra flooding events (Fig. 5c and d respectively) showed similar cases of flood peak underestimation, especially for 2007. Generally there is good agreement for the rising and falling limbs for both summers.

The time series for 5- and 10-day lead SDF forecasts have also been shown in Fig. 5 for both the Ganges (2003 and 2007) and Brahmaputra (2004 and 2007). As with the nowcasts, the 5-day forecasts show some skill in capturing the peak flows, with the 10-day lead forecast showing no skill at forecasting the peak flood of the September 20, 2003 of the Ganges (Fig. 5a). However, all the forecasts are not considerably far from the observations during the entire monsoon season. Similarly, for 2007 (Fig. 5b) all the forecasts miss the first peak but the falling and rising limbs of the monsoon season were fairly well-captured. The results for the Brahmaputra (Fig. 5c and d) are not appreciably different from the Ganges results. In particular, the peak floods of the Brahmaputra 2007 monsoon season (specifically July, 7 and September, 13), as shown in Fig. 5d, were marginally captured by the 5-day forecasts, with the 10-day lead forecasts showing essentially no skill. We examine next the forecast of the entire time series instead of just select years.

Fig. 6 presents the NS efficiency coefficient (see Eq. 2) versus lead time calculated for whole time period ranging from December 8, 1997

to December 31, 2010, which can be viewed as an error variance normalized by the climatological variance of the signal. The Nash–Sutcliffe (NS) efficiency coefficient is calculated as:

$$NS = 1 - \frac{\sum_{i=1}^N (Q_{oi} - Q_{mi})^2}{\sum_{i=1}^N (Q_{oi} - \bar{Q}_o)^2} \quad (2)$$

where Q_{oi} is observed discharge at time i , Q_{mi} is the modeled discharge at time i , and \bar{Q}_o is the mean. Note that a NS value of one means the forecast and the observations are identical, while a NS value of zero means the forecast is no better than forecasting the fixed climatological average (\bar{Q}_o). It considers the entire flow cycle but does not provide specific information on how well flood peaks or low flows are predicted, for which other metrics are more appropriate. The NS efficiency score of the 1-day lead time discharge forecast was 0.80 and declined to 0.52 for 15 day forecast in the case of the Ganges; similarly the NS for the Brahmaputra decreased from 0.80 for the 1-day forecast to 0.56 for the 15-day forecast. These NS scores show that the SDF nowcasts and forecasts capture a majority of the variability in the river discharge time-series.

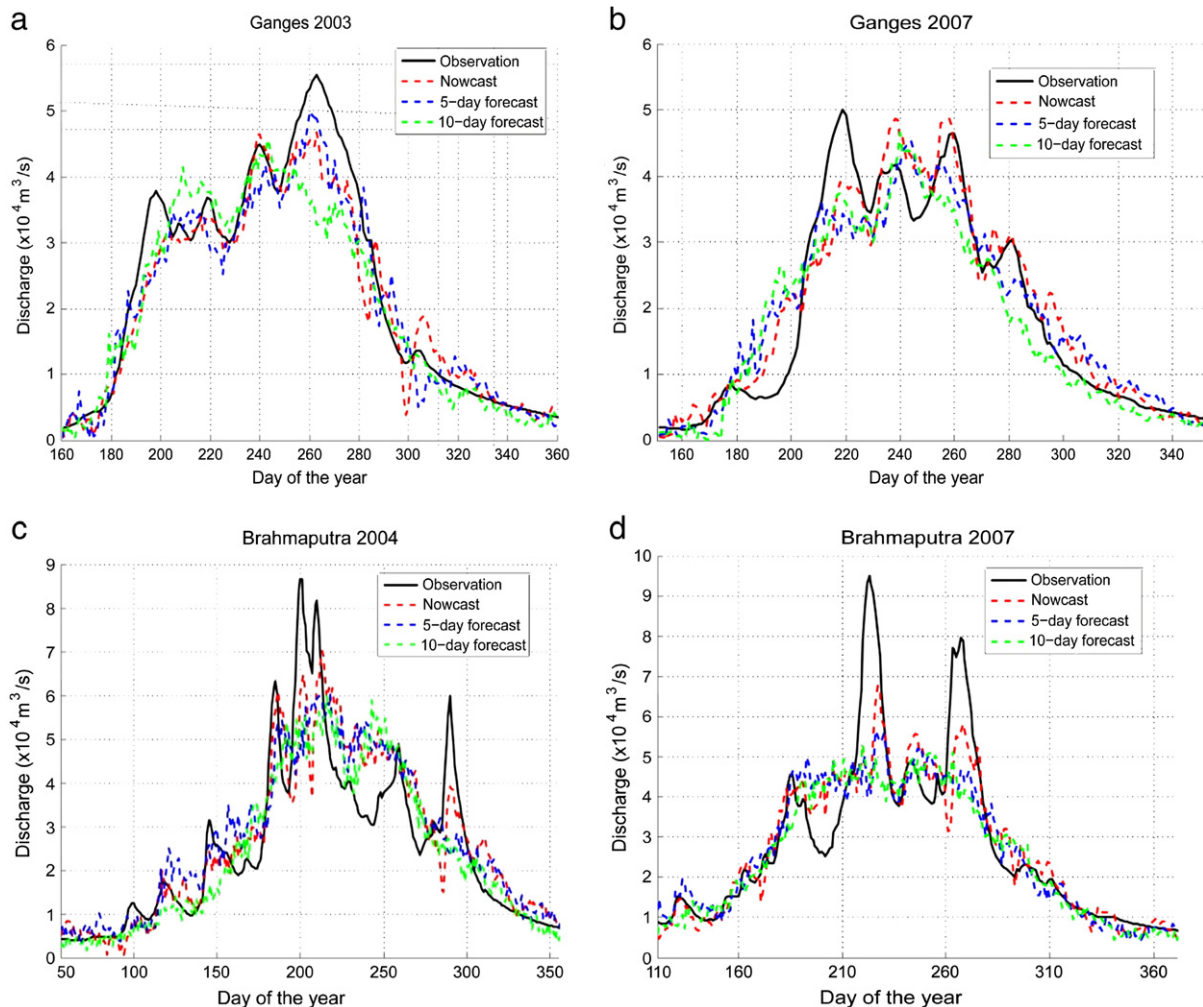


Fig. 5. Daily time series of observed river discharge, nowcast and forecast (for selected lead time) based on the river flow signal observed from satellite. The upper panels show 2003 (5a) and 2007 (5b) results for Ganges River at Hardinge bridge station in Bangladesh. The lower panels are 2004 (5c) and 2007 (5d) plots for Brahmaputra at Bahadurabad. Five and ten day lead time forecasts are selectively shown in these plots. The details of the satellite-derived flow signals used for the nowcasting have been presented in Table 1.

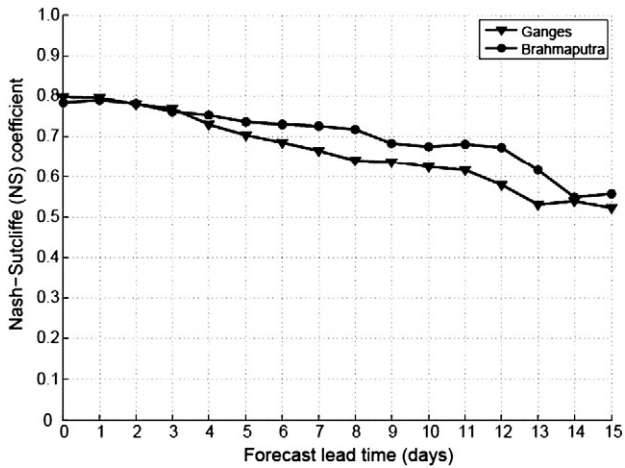


Fig. 6. The Nash–Sutcliffe coefficient versus forecast lead time for Ganges and Brahmaputra Rivers. Only satellite-derived flow signals were used for the forecast. The Nash–Sutcliffe coefficients were calculated for the whole time period of record (December 8, 1997 to December 31, 2010).

To account for optimal model changes due to seasonal variability of the river flow, we performed the cross-validation based regression separately for the dry (November–May) and wet (June–October) seasons, but there was no appreciable NS efficiency forecast skill score

improvements due to the seasonal classification. Overall, the results indicate that the remotely sensed flow signals contain useful information regarding surface water flow estimation and forecasting and could be used in these large rivers to improve river flow forecasting skill, especially if used in conjunction with other flow forecasting data.

5.2. Discharge forecasts using combined SDF signals and persistence

Now, in addition to the SDF signals, we incorporate the forecast point river gauged discharge data at the forecast initialization time into the cross-validation forecast model to examine how much the SDF improves forecast skill with respect to a persistence “forecast”. In this context, a “persistence forecast” is the gauged-based observed discharge time-lagged by the forecast lead time. This method relies on the availability of near-real-time discharge observations at the forecast point, with the expectation that the combined use of the observed discharge with the SDF should improve the forecast skill. Fig. 7 presents the daily time series of discharge forecasts for selected flood years for Ganges and Brahmaputra (similar to Fig. 5 above). The plots show that combined use of persistence and satellite information clearly improved the discharge forecast compared to satellite-only forecast presented above (Section 5.1). The RMSE for each forecast lead time is presented next.

Also on a separate step, for comparison purpose, we fit the Autoregressive Moving-Average (ARMA) model to the in-situ discharge recorded at the forecast points of the Ganges and Brahmaputra rivers. Based on the minimum Akaike Information Criteria (AIC), ARMA(7,1) has been identified as the optimal model for both rivers. The ARMA(7,1)

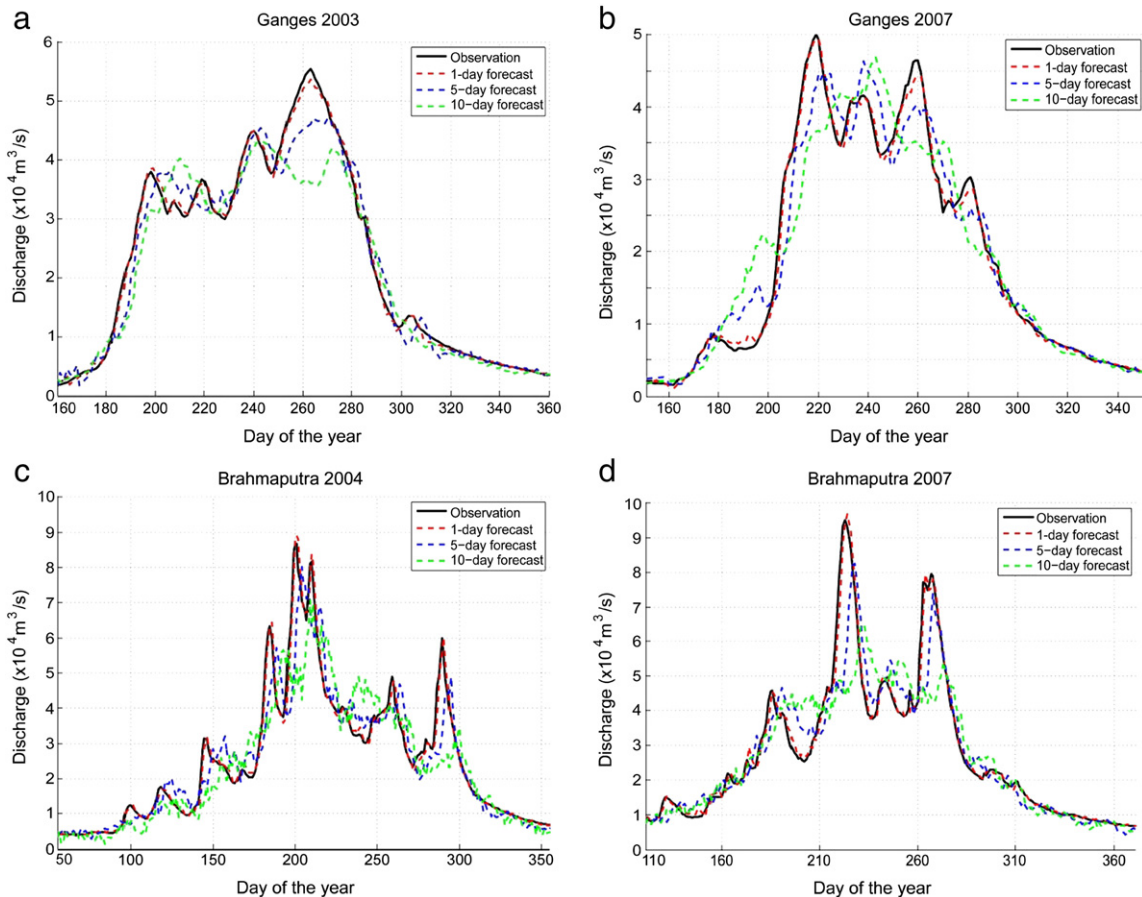


Fig. 7. Daily time series based on satellite derived signals and persistence (SDF + PERS) based river discharge forecast at selected lead times shown against observation during the 2003 (6a) and 2007 (6b) flooding of Ganges River at Hardinge bridge station in Bangladesh. The 2004 (6c) and 2007 (6d) forecasts for Brahmaputra at Bahadurabad are also shown.

refers to seven autoregressive and one moving average terms in the ARMA model.

Fig. 8a shows the RMSEs of persistence-only (PERS), ARMA, and combined SDF and persistence (SDF + PERS) forecasts for both rivers. The SDF + PERS forecast error increases with lead time ranging from 1530 m³/s (7%) for 1 day lead forecast to 8190 m³/s (37%) for 15 day lead time in the case of the Brahmaputra, and from 804 m³/s (6.4%) to 5315 m³/s (41.4%) for the Ganges. The SDF + PERS forecast has lower RMSE compared to PERS forecast for all lead times for both Ganges and Brahmaputra, and also the ARMA forecast is expectedly better than PERS. For the Brahmaputra, the SDF + PERS has considerably smaller error forecast compared to ARMA for lead times beyond 3 days indicating that the passive microwave provides useful information for discharge monitoring for the river. For the Ganges, however, the ARMA forecast is better than SDF + PERS for shorter lead times up to 10 days and slightly inferior beyond. The SDF-only nowcast (presented in Section 5.1 above) has also been indicated on Fig. 8a. on the vertical axis (zero lead time).

The contribution of the SDF signal in the improvement of the forecast skill can be shown by comparing against persistence. We further examine these comparisons through RMSE skill scores (RSS), where the RSS is calculated as

$$RSS = \frac{RMSE_f - RMSE_{pers}}{RMSE_{perf} - RMSE_{pers}}, \quad (3)$$

where $RMSE_f$ is the RMSE for the forecasts, $RMSE_{pers}$ for persistence, and $RMSE_{perf}$ for a “perfect” forecast (with a value of 0 in this case). The RMSE values for the forecast and persistence are as indicated in Fig. 8a. Fig. 8b shows the RMSE skill score of the 1 to 15 day lead SDF + PERS forecast with reference to persistence for both Ganges and Brahmaputra rivers. The RMSE skill score varies from value of 1 (forecast with perfect skill) to large negative number (forecast with no skill), and a value of 0 denotes that the forecast has no better skill than the reference forecast. The microwave derived river flow signals improved the forecast RMSE skill score of SDF + PERS from 5% to 15% for Ganges and from 7.5% to 17% for Brahmaputra across the 15 day lead time. For operational purposes, the forecast skill could be further improved through a combination of ARMA and satellite approaches; however the ARMA model requires seven (equal to number of autoregressive terms) continuous past observations for the optimal model estimated above. While this would not be a problem for sites with consistent reporting of discharge observations, it poses more challenges for operational forecasting for river reaches with intermittent reporting. Given the skill that we achieve through the use of limited observations and satellite remotely sensed information (aka SDF + PERS), this shows the power of utilizing remotely sensed information to provide additional reliable skill to river flow forecasts for reaches with reporting-limited data.

6. Water level from discharge forecast

To show the impact of SDF to enhance river stage forecasts, we converted the river discharge forecasts to water level (river stage) by inverting the flows using the rating curves, and compared them with the ground based water level measurements made by the FFWC. Fig. 9 presents the RMSE of the water level forecast produced from satellite signals and persistence (SDF + PERS) for monsoon season (June–October). As described, above (also see Fig. 8a) the discharge forecast from SDF + PERS is relatively better than those from PERS and ARMA alone, and hence from now onwards we focus on presenting the results of the SDF + PERS. The RMSE varies with forecast lead time and more importantly differs from river to river. The RMSEs computed for all days, including the low and high flow seasons, increase with forecast lead time for both rivers. And it is found that the error has consistently larger values for the Ganges compared to the Brahmaputra.

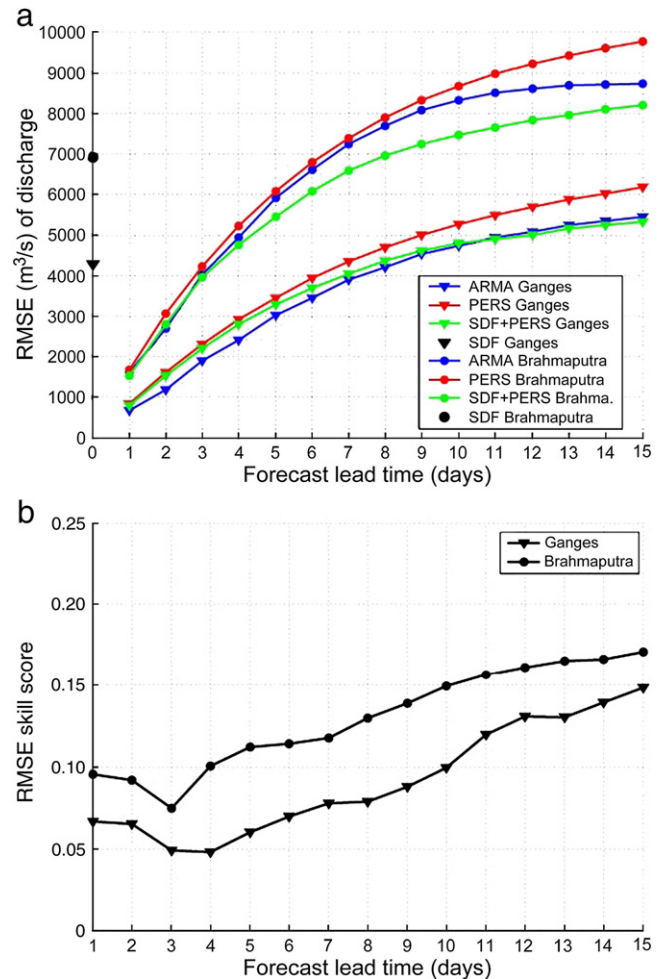


Fig. 8. a) The RMSE of persistence (PERS), Autoregressive moving-average (ARMA), and combined SDF and persistence (SDF + PERS) discharge forecasts for Ganges and Brahmaputra rivers. The SDF + PERS forecast is better than the PERS for both rivers and the ARMA expectedly beats the PERS. The SDF + PERS forecast has lower RMSE than ARMA for Brahmaputra, but this is not the case for Ganges. The SDF-only nowcasts (dark points on the vertical axis) indicates that the satellite discharge estimate (see Fig. 5) is at least as good as 7 day lead time forecast that is aided by in situ discharge. b) The root mean square error (RMSE) skill score of SDF + PERS forecast versus forecast lead time for the Ganges and the Brahmaputra Rivers discharge forecasts. The skill scores were calculated for the whole time period of record (December 8, 1997 to December 31, 2010).

One factor that could be contributing to the larger forecast error for the Ganges compared to the Brahmaputra is that the river flow extent estimated by the PMW sensors is translated to discharge (and water level) more accurately for shallower-sloped river banks (such as the Brahmaputra) than for steeper river banks, which is the relative case when comparing the banks of the Brahmaputra with the Ganges near their respective gauging locations. For rivers with shallower-sloped banks, small variations in the river discharge produce proportionally larger changes in river width and, hence, the variation can more easily be detected by the PMW sensors. The comparison of the forecast error for different flow regimes is discussed next.

The magnitude of the flow also has an impact on the accuracy of the river flow extent detected by the PMW. Fig. 10a and b denotes how the RMSE of the water level forecast for monsoon season depends on the flow magnitude for the Ganges and the Brahmaputra respectively. Note that these forecasts are made based on the combination of the SDF signals detected by PMW and persistence as discussed in the earlier sections. The SDF signals are estimated from the difference in microwave emission of water and land surfaces and are sensitive to the changes in the area of land covered with water. Therefore, it is to be

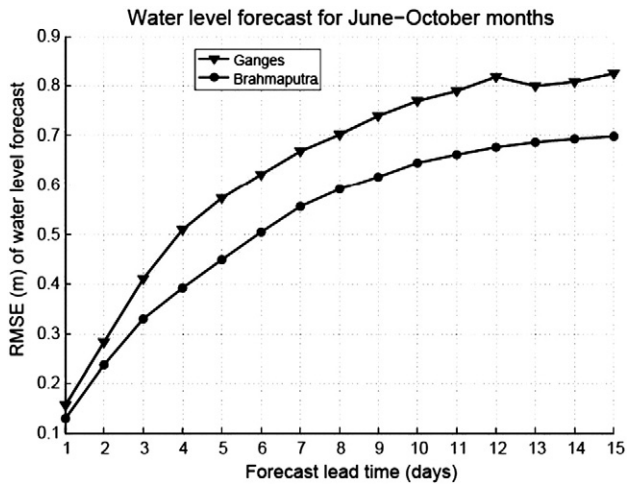


Fig. 9. Root mean square error (RMSE) of monsoon water level forecast for the Ganges and the Brahmaputra Rivers shown for different forecast lead times. The error increases with lead time for both rivers, and it is larger for the Ganges compared to the Brahmaputra.

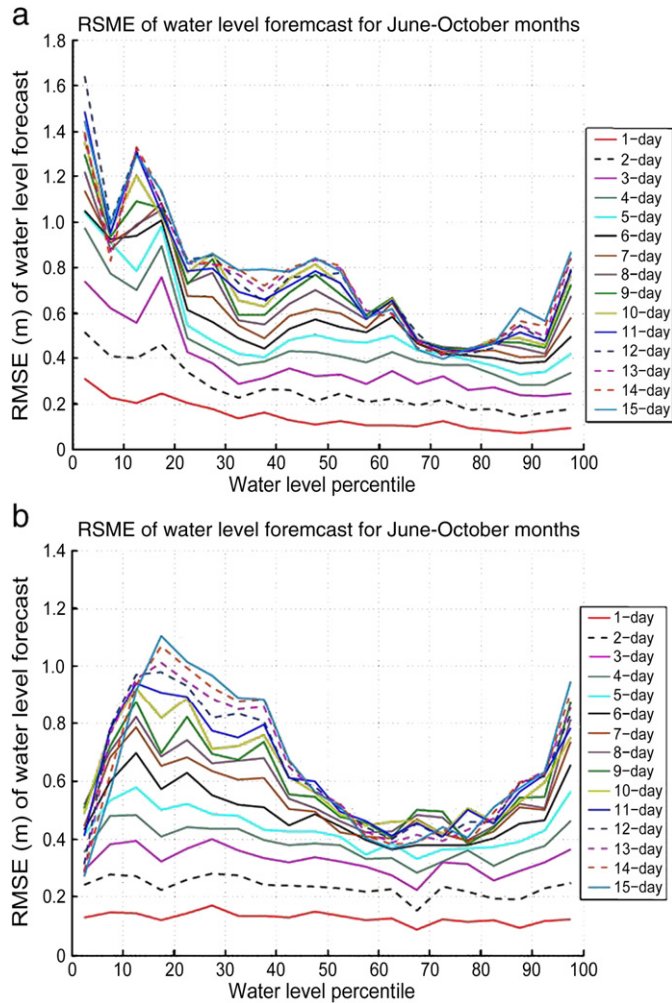


Fig. 10. a. RMSE of water level forecast for Ganges River shown for different flow regimes during monsoon season (June–October). The water level is obtained from discharge forecast using the rating curve equations. The water level forecast errors decrease with increasing flow magnitude indicating that the PMW sensors detect floods more accurately when the river overflows the bank, inundating wider area, as opposed to low flow where the flow remains in the river bank. b. Same as Fig. 10a except for Brahmaputra River.

expected that high flows have a tendency to extend over the river banks covering a large area and, as a result, a stronger river flow signal is detected. Fig. 10a confirms this scenario for the Ganges. The forecast error is higher for low flows (lower percentiles) and it has a decreasing trend with increasing flow magnitude. This is the case for all forecast lead times. Results for Brahmaputra (Fig. 10b) generally indicate similar trends: the forecast errors are smaller for high flow volumes, particularly for 50 to 90 flow percentiles of the monsoon season. The RMSE picks up for the highest flow volumes (largest percentile) due to, as seen from the time series, the fact that the peaks are mostly not captured by the forecast. The heteroscedastic behavior (particularly having bigger variance for large flows) of the gauging and rating curve errors also could contribute to the large error for the highest flow percentiles.

However, besides geomorphological considerations, another factor why the low flow Ganges errors are more appreciable than those of the Brahmaputra concerns the issue of water diversions, as discussed in Section 2. We assume that this disparity is attributed to the fact that the Ganges is affected by human influences through construction of irrigation dams and barrages for water diversions in India (Jian et al., 2009), while the Brahmaputra is less affected by man-made impacts, as there are no major hydraulic structures along its main stem as of 2010.

Overall, the PMW based water level forecast provides comparable forecast errors with satellite altimetry based forecasts (such as for example Biancamaria et al., 2011) but with the advantage of higher sampling repeat periods (1 day versus 10 days). The PMW data can be combined with altimetry based water level estimates to further improve the accuracy of river stage forecast.

7. Conclusion

This study shows that flow information derived from passive microwave remote sensing is useful for near-real time river discharge forecasting for the Ganges and Brahmaputra Rivers in Bangladesh. It presents a different approach to the satellite altimetry based water level forecast performed by Biancamaria et al. (2011). The current method uses multiple (more than 20 for each river) upstream river reach estimates from a selected frequency band of a passive microwave signal such that noise introduced by cloud cover is minimal. The remote sensing observational data (SDFs) are well correlated, albeit with different patterns between the two basins, to the ground flow measurements and are capable of tracking river flow wave propagation downstream along the rivers. The

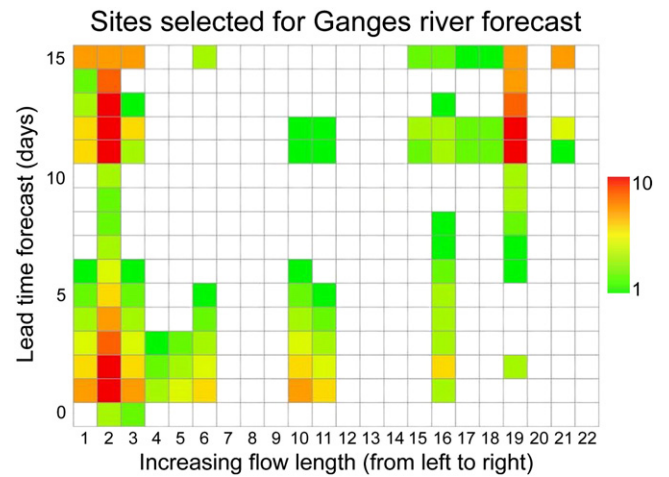


Fig. A1. Map showing the sites selected by the cross-validation regression model [Section 4 (iii)] for each lead time forecast. The numbers on the horizontal axis refer to sites as described in Table 1, with increasing FPL from left to right. Meanwhile, the numbers on the vertical axis denote the lead time forecast and the nowcast is represented by lead time of '0'. The color map shows the number of times (including the lagged observations) data from a SDF site is used in the regression model. (For interpretation of the references to color in this figure legend, the reader is referred to the web version of this article.)

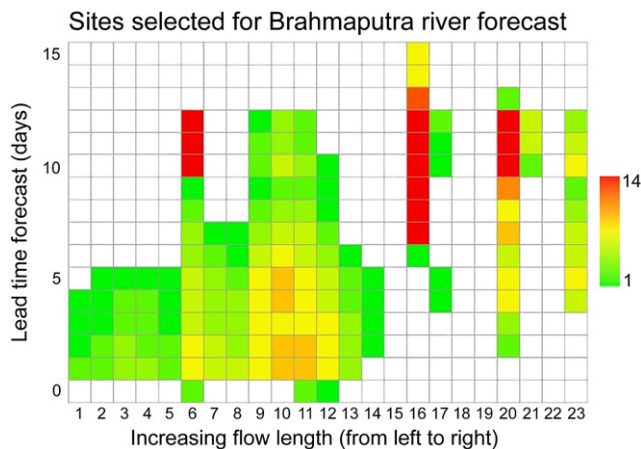


Fig. A2. Same as Fig. A1 except for Brahmaputra River.

correlation pattern depends on the location, flow path length and lead time indicating that the local ground conditions such as river geometry, topography, precipitation spatial scale, and hydrologic response of the watershed should be taken into consideration before using the satellite signal for river flow application. The relative importance and influence of each of these factors needs further exploration.

The SDF signals are used in this paper in cross-validation regression models for river flow nowcasting and forecasting at 1–15 day lead times. The skill of the forecasts improves at all lead times compared to persistence for both Ganges and Brahmaputra Rivers. The forecast error is smaller for the Brahmaputra compared to the Ganges, and also the accuracy improves for high flow magnitudes for both Rivers. This makes a substantial proof of utility of passive microwave remote sensing for flood forecast applications in data-scarce regions. However we should point out that one needs to identify the appropriate locations where the river width estimates are correlated with the gauge measurements before using them for such applications. When the river flow is confined and the discharge variations mainly results in water level change, the information obtained from river width estimates may not be useful to detect the magnitude of river flows, in which case altimetry water level data is the better option. However, the PMW of the frequency band minimizes cloud cover effects, allowing daily observations, which is not currently possible for altimetry data. It is clear that passive microwave remote sensing of river discharge can play a useful role in measurements of upstream flow variation, and as a river flow measurement, it would be useful to couple with hydrologic models in a data assimilation and model calibration framework for river flow forecasting purposes.

Acknowledgments

The first author was supported by NASA Earth and Space Science Fellowship. He is also thankful to the Center for Environmental Sciences and Engineering (CESE) of the University of Connecticut for the partial financial support through 'CESE 2010–11 Graduate Student Research Assistantships' and 'Multidisciplinary Environmental Research Award, 2010–2011'. We are grateful for the Flood Forecasting and Warning Center of Bangladesh for providing the river stage data used in this project, and for the assistance of Jennifer Boehnert with GIS support. We also gratefully acknowledge NASA grant NNX12AQ34G which partially supported this research. The paper greatly benefited from inputs of three anonymous reviewers.

Appendix A. Sites selected using cross-validation model

For each forecast lead time, the sites selected by the cross-validation approach, described earlier under Section 4 (iii), are presented in Figs. A1 and A2 for Ganges and Brahmaputra respectively. For the Ganges

(Fig. A1), twelve out of the total of 22 sites have not been used at all for 0–10 days lead time forecast, and a maximum of 3 sites were used for 7–10 days lead time forecast. Note that the forward-selection cross-validation approach selects which sites produce the “best forecast” based on the minimized least square error. Almost all of the downstream sites (with exception of a few stations) in India were included for short time forecasts of the Brahmaputra, while some of the upstream sites located in China were used for long lead times. The cross-validation model completely disregards the 5 downstream sites for forecast lead times beyond 5 days. The middle sites, particularly “11579 (9)” to “11583” (11) were chosen for up to 13 day lead time forecast. Overall, four out of a total of 23 sites were not used at all for any forecast or nowcast of the Brahmaputra.

References

- Alsdorf, D. E., Melack, J. M., Dunne, T., Mertes, L., Hess, L., & Smith, L. C. (2000). Interferometric radar measurements of water level changes on the Amazon floodplain. *Nature*, *404*, 174–177.
- Alsdorf, D. E., Smith, L. C., & Melack, J. M. (2001). Amazon floodplain water level changes measured with interferometric SIR-C radar. *IEEE Transactions on Geoscience and Remote Sensing*, *39*, 423–431.
- Beven, K. J. (1979). Generalized kinematic routing method. *Water Resources Research*, *15*(5), 1238–1242.
- Biancamaria, S., Hossain, F., & Lettenmaier, D. (2011). Forecasting transboundary flood with satellites. *Geophysical Research Letters*, *38*, L11401. <http://dx.doi.org/10.1029/2011GL047290>.
- Birkett, C. M. (1998). Contribution of the TOPEX NASA radar altimeter to the global monitoring of large rivers and wetlands. *Water Resources Research*, *34*(5), 1223–1239.
- Birkinshaw, S. J., O'Donnell, G. M., Moore, P., Kilsby, C. G., Fowler, H. J., & Berry, P. A. M. (2010). Using satellite altimetry data to augment flow estimation techniques on the Mekong River. *Hydrological Processes*. <http://dx.doi.org/10.1002/hyp.7811>.
- Bjerkle, D. M., Moller, D., Smith, L. C., & Dingman, S. L. (2005). Estimating discharge in rivers using remotely sensed hydraulic information. *Journal of Hydrology*, *309*, 191–209.
- Brakenridge, G. R., Nghiem, S. V., Anderson, E., & Chien, S. (2005). Space-based measurement of river runoff. *EOS, Transactions of the American Geophysical Union*, *86*(19), 185–188.
- Brakenridge, G. R., Nghiem, S. V., Anderson, E., & Mic, R. (2007). Orbital microwave measurement of river discharge and ice status. *Water Resources Research*, *43*, W04405. <http://dx.doi.org/10.1029/2006WR005238>.
- Brakenridge, G. R., Tracy, B. T., & Knox, J. C. (1998). Orbital SAR remote sensing of a river flood wave. *International Journal of Remote Sensing*, *19*(7), 1439–1445.
- CEGIS (2006a). *Sustainable end-to-end climate/flood forecast application through pilot projects showing measurable improvements*. CEGIS Base Line Rep (78 pp.).
- CEGIS (2006b). *Early warning system study: Final report*. Asian Development Bank (100 pp.).
- Chow, V. T., Maidment, D. R., & Mays, L. W. (1988). *Applied hydrology*. New York: McGraw-Hill (572 pp.).
- De Groeve, T. (2010). Flood monitoring and mapping using passive microwave remote sensing in Namibia. *Geomatics, Natural Hazards and Risk*, *1*(1), 19–35.
- De Groeve, T., Kugler, Z., & Brakenridge, G. R. (2006). Near real time flood alerting for the global disaster alert and coordination system. In B. Van De Walle, P. Burghardt, & C. Nieuwenhuis (Eds.), *Proceedings ISCRAM2007* (pp. 33–39). Newark, NJ: ISCRAM.
- Flood Forecasting and Warning Centre (2000). Personal communication.
- GDACS, Global Disaster Alert and Coordination System (2011). *Global Flood Detection System*. <http://www.gdacs.org/floodmerge/>
- Gupta, H. V., Harald, K., Yilmaz, K. K., & Guillermo, F. M. (2009). Decomposition of the mean squared error and NSE performance criteria: Implications for improving hydrological modeling. *Journal of Hydrology*, *377*, 80–91.
- Hopson, T. M., & Webster, P. J. (2010). A 1–10-day ensemble forecasting scheme for the major river basins of Bangladesh: Forecasting severe floods of 2003–07. *Journal of Hydrometeorology*, *11*, 618–641. <http://dx.doi.org/10.1175/2009JHM1006.1>
- Huffman, G. J., Adler, R. F., Curtis, S., Bolvin, D. T., & Nelkin, E. J. (2005). Global rainfall analyses at monthly and 3-hr time scales. In V. Levizzani, P. Bauer, & J. F. Turk (Eds.), *Measuring precipitation from space: EURAINSAT and the future*. Springer (722 pp.).
- Huffman, G. J., et al. (2007). The TRMM multisatellite precipitation analysis (TMPA): Quasi-global, multiyear, combined sensor precipitation estimates at fine scales. *Journal of Hydrometeorology*, *8*, 38–55.
- Jian, J., Webster, P. J., & Hoyos, C. D. (2009). Large-scale controls on Ganges and Brahmaputra river discharge on intraseasonal and seasonal time-scales. *Quarterly Journal of the Royal Meteorological Society*, *135*(639), 353–370.
- Joyce, R. J., Janowiak, J. E., Arkin, P. A., & Xi, P. (2004). CMORPH: A method that produces global precipitation estimates from passive microwave and infrared data at high spatial and temporal resolution. *Journal of Hydrometeorology*, *5*, 487–503.
- Jung, H. C., Hamski, J., Durand, M., Alsdorf, D., Hossain, F., Lee, H., et al. (2010). Characterization of complex fluvial systems via remote sensing of spatial and temporal water level variations. *Earth Surface Processes and Landforms, SPECIAL ISSUE-Remote Sensing of Rivers*. <http://dx.doi.org/10.1002/espl>.
- Kugler, Z., & De Groeve, T. (2007). *The global flood detection system*. Luxembourg: Office for Official Publications of the European Communities.

- Papa, F., Durand, F., Rossow, W. B., Rahman, A., & Balla, S. K. (2010). Satellite altimeter-derived monthly discharge of the Ganga-Brahmaputra River and its seasonal to interannual variations from 1993 to 2008. *Journal of Geophysical Research*, 115, C12013. <http://dx.doi.org/10.1029/2009JC006075>.
- RIMES (2008). *Background paper on assessment of the economics of early warning systems for disaster risk reduction*. RIMES/ADPC Report to The World Bank Group, GFDRR (69 pp.).
- Siddique-E-Akbor, A. H., Hossain, F., Lee, H., & Shum, C. K. (2011). Inter-comparison study of water level estimates derived from hydrodynamic-hydrologic model and satellite altimetry for a complex deltaic environment. *Remote Sensing of Environment*, 115, 1522–1531. <http://dx.doi.org/10.1016/j.rse.2011.02.011>.
- Singh, V. P., Sharma, N., & Ojha, C. S. P. (2004). *Brahmaputra basin water resources*. *Water Science and Technology Library Series, Vol. 47*, The Netherlands: Kluwer Academic Publishers (632 pp.).
- Smith, L. C. (1997). Satellite remote sensing of river inundation area, stage and discharge: A review. *Hydrological Processes*, 11, 1427–1439.
- Smith, L. C., & Pavelsky, T. M. (2008). Estimation of river discharge, propagation speed, and hydraulic geometry from space: Lena River, Siberia. *Water Resources Research*, 44, W03427. <http://dx.doi.org/10.1029/2007WR006133>.
- Temimi, M., Leconte, R., Brissette, F., & Chaouch, N. (2005). Flood monitoring over the Mackenzie River Basin using passive microwave data. *Remote Sensing of Environment*, 98, 344–355.
- Woldemichael, A. T., Degu, A. M., Siddique-E-Akbor, A. H. M., & Hossain, F. (2010). Role of land-water classification and Manning's roughness parameter in space-borne estimation of discharge for braided rivers: A case study of the Brahmaputra River in Bangladesh. *IEEE Special Topics in Applied Remote Sensing and Earth Sciences*. <http://dx.doi.org/10.1109/JSTARS.2010.2050579>.